

A Space-Time Approach for the Time-Domain Simulation in a Rotating Reference Frame

M. Klimek* S. Kurz*,† S. Schöps*,† T. Weiland†

Abstract—We approach the discretisation of Maxwell’s equations directly in space-time without making any non-relativistic assumptions with the particular focus on simulations in rotating reference frames. As a research example we study Sagnac’s effect in a rotating ring resonator. After the discretisation, we express the numerical scheme in a form resembling 3D FIT with leapfrog. We compare the stability and convergence properties of two 4D approaches, namely FIT and FEM, both using Whitney interpolation.

I. INTRODUCTION

Concerning Clifford’s Geometric Algebra, we use the nomenclature and notation of [5], which we also perceive as a comprehensive introduction to this mathematical formalism. Maxwell’s equations [5, Eq. (7.39)] read

$$\nabla \wedge F = 0, \quad \nabla \cdot G = J, \quad (1)$$

where F (or G) is the (dual) Faraday bivector, and J the space-time current vector.

The bivectors F and G are related by constitutive material mapping ξ defined implicitly by

$$G = \xi(F). \quad (2)$$

For linear, isotropic media ξ is a space-time generalisation of the well known constitutive equations. To derive an explicit formula for ξ , we start with

$$\vec{D} = \varepsilon \vec{E} \quad \text{and} \quad \vec{H} = \nu \vec{B}, \quad (3)$$

where $\varepsilon, \nu, \vec{E}, \vec{H}, \vec{D}, \vec{B}$ are electric permittivity, magnetic reluctance, electric and magnetic field strengths,

* Graduate School of Computational Engineering, Technische Universität Darmstadt, Dolivostraße 15, D-64293, Darmstadt, Germany, e-mail: klimek@gsc.tu-darmstadt.de, tel.: +49 6151 16-24391, fax: +49 6151 16-24404.

† Institut für Theorie Elektromagnetischer Felder, Technische Universität Darmstadt, Schlossgartenstraße 8, D-64289, Darmstadt, Germany, e-mail: thomas.weiland@temf.tu-darmstadt.de

and fluxes, respectively. The resulting expression is given by

$$\xi(F) = \frac{1}{2} \left[\left(\varepsilon + \frac{\nu}{c^2} \right) F - \left(\varepsilon - \frac{\nu}{c^2} \right) u F u \right], \quad (4)$$

with u the four-velocity vector of the material, and c the speed of light in vacuum.

II. MOTION AS MESH’S GEOMETRY

Motion of the system is modelled by specifying Lagrangian placement map $p_t(\vec{r}_{\text{ref}})$, which gives a space-time position (at time t) of a particle with initial position \vec{r}_{ref} . The cylindrical coordinates of \vec{r}_{ref} are denoted by r, φ, z . For a system rotating with constant angular velocity Ω around z -axis we use

$$p_t(\vec{r}_{\text{ref}}) = [t, r \cos(\theta), r \sin(\theta), z], \quad (5)$$

with $\theta = \varphi + \tanh(r\Omega/c) ct/r$.

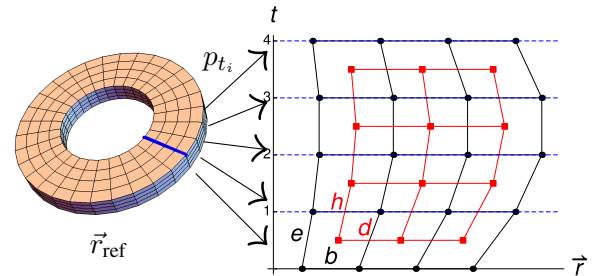


Fig. 1. Sketch of a space-time mesh used in simulation. The thick blue line in the left image is mapped to horizontal lines in the right figure.

We extrude a 3D mesh by applying p_{t_i} to nodes’ positions for all time steps t_i and connecting the 4D nodes stemming from the same 3D node; see Fig. 1. By K_n^i (respectively \tilde{K}_n^i) we denote the i -th n -dimensional element of the (barycentric dual) mesh.

III. DISCRETIZATION

Maxwell's equations (1) are discretised by applying their integral form to the primal/dual mesh pair, i.e.,

$$\oint_{\partial K_3^i} (d^2x) \cdot F = 0, \quad \oint_{\partial \tilde{K}_3^i} (d^2x) \wedge G = \int_{\tilde{K}_3^i} (d^3x) \wedge J, \quad (6)$$

and introducing scalar DoFs (Degrees of Freedom) on the primal mesh

$$f_j := \int_{K_2^j} (d^2x) \cdot F, \quad (7)$$

and analogously for the dual mesh. Next, we rename and renumber the DoFs on the primal mesh as follows

$$f_j =: \begin{cases} e_l^{n+1/2} & \text{if } K_2^j \text{ is timelike,} \\ b_m^n & \text{if } K_2^j \text{ is spacelike,} \end{cases} \quad (8)$$

where the relation between the indices j, l, m and n is as follows (see also Fig. 2). If the facet K_2^j is timelike, it is the edge l in the reference mesh M^3 extruded in time via the placement map p_t such that $t \in [t_n, t_{n+1}]$. Similarly, if the facet K_2^j is spacelike, then it is the image of a facet with index m in M^3 under the map p_t with $t = t_n$. Analogously on the dual mesh, we split g_j into $d^{n-1/2}$ and h^n .

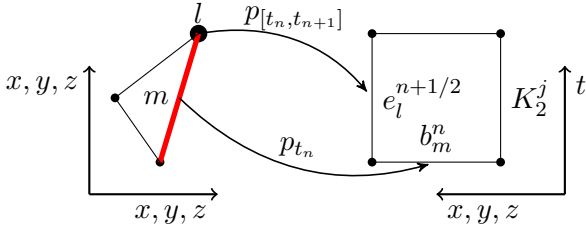


Fig. 2. Illustration of the relation between indices in (8). The leftmost is the reference mesh. The l -th edge is depicted as a fat dot, and m -th 2D facet as a thick red line. The rightmost is the space-time mesh. 2D facets are depicted as lines.

A. Material Equations

A discrete equivalent of ξ in (4) is a material matrix M_ξ relating discrete equivalents of F and G , i.e.,

$$g_i = \sum_j [M_\xi]_{ij} f_j. \quad (9)$$

In both methods described below, we use n -vector valued Whitney interpolating functions N_i^n associated with i -th n -dimensional element of the mesh to derive explicit expressions for M_ξ .

1) *4D FEM*: Applying energetic approach [4] also known as Galerkin Hodge star [3], we arrive at the material matrix with entries

$$[M_\xi^{\text{FEM}}]_{jk} := \int_{K_4} N_j^2 \cdot \xi(N_k^2) |d^4x|. \quad (10)$$

2) *4D FIT*: The 4D FIT material matrix with Whitney interpolation written using Geometric Algebra reads

$$[M_\xi^{\text{FIT}}]_{jk} := I^{-1} \widetilde{W}_j \wedge \bar{\xi}_j (N_k^2(x_j)), \quad (11)$$

with $\bar{\xi}_j$ is ξ averaged over the j -th dual facet, and \widetilde{W}_j the bivector associated with it, describing its magnitude and orientation in space-time. Although the collocation point x_j may be chosen arbitrarily, we choose the barycenter of K_2^j due to ease of calculation.

3) *Reduction to 3D Material Matrices and their Symmetrisation*: The material matrix M_ξ is split into 3D material matrices $M_{\varepsilon/\nu, e/b}^\pm$ to resemble a 3D time marching scheme. E.g., $M_{\varepsilon^+}^+$ is the block of M_ξ relating $d^{n+1/2}$ (role of ε) to the future (role of $+$) magnetic b DoF (role of b), i.e., b^{n+1} .

While M_ξ^{FEM} is symmetric by construction (10), the FIT material matrix M_ξ^{FIT} is symmetrised in order to avoid instabilities, as explained in [6, especially Sec. II]. The symmetrisation of M_ξ^{FIT} translates to the following redefinitions, where M^T is the transpose of M ,

$$M_{\nu b}^{\text{FIT, sym}} := \frac{1}{2} \left(M_{\nu b}^{\text{FIT}} + [M_{\nu b}^{\text{FIT}}]^T \right) \quad (12)$$

$$M_{\varepsilon \varepsilon}^{\text{FIT, sym}} := \frac{1}{2} \left(M_{\varepsilon \varepsilon}^{\text{FIT}} + [M_{\varepsilon \varepsilon}^{\text{FIT}}]^T \right) \quad (13)$$

$$M_{\varepsilon b}^{\pm \text{FIT, sym}} := \frac{1}{2} \left(M_{\varepsilon b}^{\pm \text{FIT}} + [M_{\nu e}^{\mp \text{FIT}}]^T \right) \quad (14)$$

$$M_{\nu e}^{\pm \text{FIT, sym}} := \frac{1}{2} \left(M_{\nu e}^{\pm \text{FIT}} + [M_{\varepsilon b}^{\mp \text{FIT}}]^T \right) \quad (15)$$

$$M_{\nu b}^{\pm \text{FIT, sym}} := \frac{1}{2} \left(M_{\nu b}^{\pm \text{FIT}} + [M_{\nu b}^{\mp \text{FIT}}]^T \right). \quad (16)$$

B. Resulting System of Linear Equations

We have split space-time material matrix and DoFs into their 3D counterparts in a way, that the obtained numerical scheme resembles 3D FIT with leapfrog, i.e.,

$$\begin{aligned} h^n &= M_{\nu b}^- b^{n-1} + M_{\nu e}^- e^{n-1/2} + M_{\nu b}^+ b^n \\ &\quad + M_{\nu e}^+ e^{n+1/2} + M_{\nu b}^+ b^{n+1} \\ d^{n+1/2} &= d^{n-1/2} + \tilde{C} h^n \\ e^{n+1/2} &= M_{\varepsilon \varepsilon}^{-1} \left[d^{n+1/2} - M_{\varepsilon b}^- b^n - M_{\varepsilon b}^+ b^{n+1} \right] \\ b^{n+1} &= b^n + C e^{n+1/2}. \end{aligned} \quad (17)$$

We would like to note, that if $\Omega = 0$ then all material matrices except $M_{\varepsilon e}$ and $M_{\nu b}$ vanish, and on Cartesian grid the 4D FIT is naturally related to 3D FIT with leapfrog.

IV. STABILITY

Starting from (17) we derive the recursive formula

$$\begin{bmatrix} b^{n+1} \\ e^{n+1/2} \\ b^n \end{bmatrix} = U^n \begin{bmatrix} b^1 \\ e^{1/2} \\ b^0 \end{bmatrix}, \quad (18)$$

where U is the update matrix

$$U := \begin{bmatrix} 1 + CM^{-1}\gamma & CM^{-1}\beta & CM^{-1}\alpha \\ M^{-1}\gamma & M^{-1}\beta & M^{-1}\alpha \\ 1 & 0 & 0 \end{bmatrix}, \quad (19)$$

where 0 and 1 above are zero and identity matrices of proper dimensions and

$$\begin{aligned} M &:= M_{\varepsilon e} - \tilde{C}M_{\nu e}^+ - \tilde{C}M_{\nu b}^+C + M_{\varepsilon b}^+C \\ \alpha &:= M_{\varepsilon b}^- + \tilde{C}M_{\nu b}^- \\ \beta &:= M_{\varepsilon e} + \tilde{C}M_{\nu e}^- \\ \gamma &:= \tilde{C}M_{\nu b} + \tilde{C}M_{\nu b}^+ - M_{\varepsilon b}^-. \end{aligned}$$

The solution vector $[b^n, e^{n-1/2}]$ will stay bounded if the modulus of all eigenvalues λ of U is less or equal to unity, $|\lambda| \leq 1$. For both methods considered, the greatest $|\lambda|$ calculated on exemplary meshes used in simulations is at most 1.

As another test of stability, we initialise the solver with randomly generated initial values and observe that the norm of the solution does not grow in time.

V. CONVERGENCE

In order to verify the convergence of the scheme, we simulate the first six, $m = 0 \dots 5$, eigenmodes of the ring resonator structure studied in [1, Section IV], and compare the rotation induced frequency shift $\delta\omega^{\text{sim}}$ extracted from our numerical simulation with the non-relativistic semi-analytic approximation, [1, Eq. (4.5)], $\delta\omega^{\text{anal}} = m\Omega$. As depicted in Fig. 3 both approaches agree well in a non-relativistic regime. However, in relativistic cases the relative difference

$$\eta := \frac{|\delta\omega^{\text{sim}} - \delta\omega^{\text{anal}}|}{|\delta\omega^{\text{anal}}|} \quad (20)$$

between two approaches becomes significant, see Table I. We expect our solution to be correct as we have not made any non-relativistic assumptions as opposed to [1].

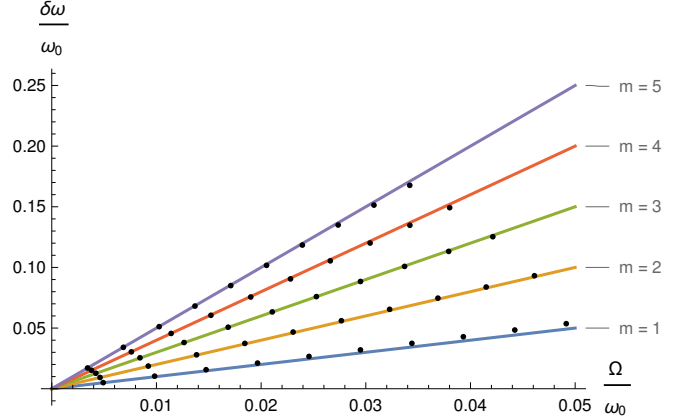


Fig. 3. Comparison of analytical (solid lines) and numerical (points) frequency shifts in case of non-relativistic velocities.

m	v_{\max}/c					
	$< 100\%$	99.63%	30.42%	3.14%	0.31%	0.03%
1	95.7%	58.1%	2.2%	0.0%	0.2%	3.2%
2	95.8%	58.5%	2.8%	0.9%	0.9%	1.0%
3	95.8%	59.2%	2.6%	2.0%	3.9%	3.4%
4	96.0%	60.6%	4.6%	1.3%	1.3%	2.4%
5	96.2%	62.2%	5.0%	8.2%	8.2%	2.6%

TABLE I

FIT CASE: THE RELATIVE DIFFERENCE η VS. MODE NUMBER AND ROTATION RATE/VELOCITY OF THE OUTER RIM OF THE RING

A. 3D Wave Simulation without Rotation

The requirements of the convergence proof in [2] are neither fulfilled by $M_{\xi}^{\text{FIT,sym}}$ nor by M_{ξ}^{FIT} (due to asymmetry). Since this is the feature of the proposed method itself, rather than its space-time extension, we focus now on 3D wave-simulation in the non-rotating ring resonator. We investigate the convergence by comparing results obtained using 4D FIT material matrix $M_{\xi}^{\text{FIT,sym}}$ with the ones using M_{ξ}^{FEM} , for which the proof [2] holds. We use temporal L^2 norm of a function of time $w : t \mapsto w(t)$

$$\|w\|_2 := \sqrt{\int_{t_{\min}}^{t_{\max}} dt [w(t)]^2}, \quad (21)$$

to define the relative difference

$$\text{diff}(E_1^z, E_2^z) := \frac{\|E_2^z(\vec{r}_{\text{sample}}) - E_1^z(\vec{r}_{\text{sample}})\|_2}{\|E_1^z(\vec{r}_{\text{sample}})\|_2}, \quad (22)$$

where $E_1^z(\vec{r}_{\text{sample}})$ is the time signal at the sample point \vec{r}_{sample} , obtained via interpolation of DoFs calculated using method and mesh indexed as 1.

The results for a (non-)orthogonal mesh, left (right) in Fig. 4, are depicted in top (bottom) of Fig. 5.

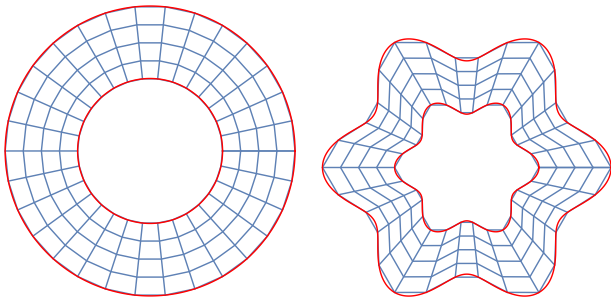


Fig. 4. Orthogonal (left) and non-orthogonal (right) mesh.

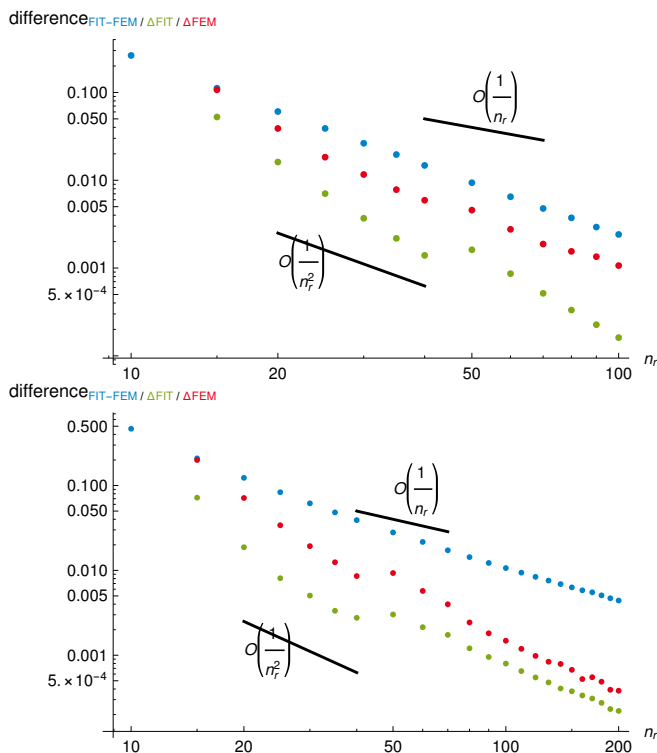


Fig. 5. The relative difference (22) between two successive FIT (green), FEM (red), and FIT and FEM (blue) solutions on the mesh with n_r nodes per wavelength. Top: (Bottom:) results obtained for (non-)orthogonal mesh, left (right) in Fig. 4.

The proof [2] can be applied to FEM independently of orthogonality of the mesh, therefore the convergence of FEM in both parts of Fig. 5 is in accordance with that theory. In case of orthogonal grid M_ξ^{FIT} is diagonal, thus symmetric, and the proof [2] can be applied in this particular situation. Although, on non-orthogonal meshes the proof [2] cannot be repeated, we observe that $M_\xi^{\text{FIT, sym}}$ gives a solution that converges to the same solution as FEM (and with a similar rate of convergence).

VI. CONCLUSION

We have applied space-time discretisation in two flavours, namely 4D FIT and FEM, without making any non-relativistic approximations. As a verification we recovered with good accuracy the rotation induced frequency shifts of the rotating ring resonator predicted by an alternative non-relativistic approach. The material matrix of our proposed extension of FIT is symmetrised to avoid instabilities. With taking only the symmetric part of the material matrix, the convergence is not guaranteed. However, we investigated numerically that FIT converges to the same solution as FEM, which is known to converge.

ACKNOWLEDGMENTS

The work of the first, second and third author is supported by the 'Excellence Initiative' of the German Federal and State Governments and the Graduate School of CE at Technische Universitaet Darmstadt.

REFERENCES

- [1] B. Z. Steinberg, A. Shamir, and A. Boag. Two-dimensional Green's function theory for the electrodynamics of a rotating medium. *Phys. Rev. E*, 74:016608, Jul 2006.
- [2] A. Bossavit. "Generalized Finite Differences" in Computational Electromagnetics. *PIER*, 32:45–64, 2001.
- [3] Computational electromagnetism and geometry. (5): The "Galerkin Hodge". *The Japan Society of Applied Electromagnetics and Mechanics*, Vol. 8, No. 2, 203–209, 2000.
- [4] L. Codecasa and F. Trevisan. Piecewise uniform bases and energetic approach for discrete constitutive matrices in electromagnetic problems. *International Journal for Numerical Methods in Engineering*, 65(4):548–565, 2006.
- [5] C. Doran and A. Lasenby. *Geometric Algebra for Physicists*. Cambridge University Press, Cambridge, second edition, 2003.
- [6] R. Schuhmann and T. Weiland. Stability of the FDTD Algorithm on Nonorthogonal Grids Related to the Spatial Interpolation Scheme. *IEEE Transactions on Magnetics*, Vol. 34, No. 5, 2751–2754, September 1998.